This article has an erratum available at: https://dx.doi.org/10.21037/tcr-22-203 and the article has been update on 2022-01-28 at here.

Original Article

Low-dose spectral CT perfusion imaging of lung cancer quantitative analysis in different pathological subtypes

Mai-Lin Chen[#], Yi-Yuan Wei[#], Xiao-Ting Li, Li-Ping Qi, Ying-Shi Sun

Key Laboratory of Carcinogenesis and Translational Research (Ministry of Education), Department of Radiology, Peking University Cancer Hospital & Institute, Beijing, China

Contributions: (I) Conception and design: YS Sun, ML Chen; (II) Administrative support: YS Sun; (III) Provision of study materials or patients: ML Chen, YY Wei; (IV) Collection and assembly of data: ML Chen, YY Wei; (V) Data analysis and interpretation: ML Chen, YY Wei, XT Li, LP Qi; (VI) Manuscript writing: All authors; (VII) Final approval of manuscript: All authors.

[#]These authors contributed equally to this work.

Correspondence to: Ying-Shi Sun. No. 52 Fu Cheng Road, Hai Dian District, Beijing, 100142, China. Email: sys27@163.com.

Background: To explore the value of the quantitative parameters of low-dose computed tomography (CT) perfusion in the diagnosis of lung cancers of different pathological types.

Methods: Eighty-five patients with lung cancer confirmed by pathology underwent enhanced spectral CT imaging with a General Electric (GE) Revolution Xtream CT scanner, including 7 patients with lung squamous cell carcinoma, 8 patients with small cell carcinoma, 67 patients with lung adenocarcinoma, and 3 patients with other pathologies. The low-dose CT perfusion parameters [blood flow (BF), blood volume (BV), time of arrival (IRF TO), maximum slope of increase (MSI), mean transit time (MTT), positive enhancement integral (PEI), time to peak (TTP) and time to maximum (Tmax)] were calculated and compared among the first three groups. One-way analysis of variance (ANOVA) or the Kruskal-Wallis test was used to compare the quantitative parameters among the three groups, and the Bonferroni method was used to correct for multiple comparisons.

Results: Among the quantitative parameters, MSI was significantly different among the three lung cancers (adenocarcinoma *vs.* squamous cell carcinoma *vs.* small cell carcinoma: 11.37±8.74 *vs.* 2.35±0.88 *vs.* 1.40±0.26, respectively; P=0.016). The MSI of lung adenocarcinoma was lower than that of non-adenocarcinoma (P=0.001), and the MSI of small cell carcinoma was lower than that of non-small cell carcinoma (P=0.014). There were no significant differences in the other parameters among these three groups (P>0.05).

Conclusions: Low-dose CT perfusion parameters may have a certain value in classifying the pathological type of lung cancer.

Keywords: Computed tomography (CT); perfusion; lung cancer

Submitted Dec 23, 2020. Accepted for publication Apr 23, 2021.
doi: 10.21037/tcr-20-3479
View this article at: https://dx.doi.org/10.21037/tcr-20-3479

Introduction

At present, the diagnosis of pulmonary nodules by conventional noninvasive computed tomography (CT) of the chest is widely performed based on their morphological characteristics and the degree of enhancement. However, there is some overlap in the morphology and enhancement of different lung nodules (1) and the ability to discriminate lung cancer from these nodules is limited. It is even more difficult to pathologically differentially diagnose different pathological types of lung cancer. In clinical practice, histopathology is the gold standard for the qualitative diagnosis of pulmonary nodules. Usually, it is necessary to use invasive modalities, such as fluoroscopically guided bronchoscopy-transbronchial biopsy (TBB) and percutaneous transthoracic needle lung biopsy (PTNB), to acquire lesion cells or tissues and achieve cytological, histological, immunohistochemical or molecular

pathological diagnosis. However, some pathological results may not be available because of the physical intolerance of certain patients to these invasive methods. Therefore, the use of noninvasive imaging methods to infer the potential histopathological type of lung nodules has been a popular research topic in recent years. CT perfusion imaging is a noninvasive functional imaging technique that reflects the hemodynamic alterations in lung nodules (2,3) via quantitative analysis involving multiple parameters, including blood flow (BF), blood volume (BV), time of arrival (IRF TO), maximum slope of increase (MSI), mean transit time (MTT), permeability surface area product (PS), positive enhancement integral (PEI), time to peak (TTP), and time to maximum (Tmax). This technique can yield a new CT imaging mode for objectively evaluating the hemodynamic characteristics of pulmonary nodules and provide a new method to assess lung lesions (3).

The purpose of this study was to investigate the value of CT perfusion imaging parameters (BF, BV, IRF TO, MSI, MTT, PS, PEI, TTP and Tmax) to pathologically differentially diagnose the different types of lung cancer. We present the following article in accordance with the MDAR checklist (available at https://dx.doi.org/10.21037/tcr-20-3479).

Methods

Patients

The study was conducted in accordance with the Declaration of Helsinki (as revised in 2013). This prospective study was approved by the Medical Ethics Committee of Peking University Cancer Hospital & Institute (NO.: 2021KT04), and written informed consent was obtained from all patients. We analyzed a total of 85 patients from Peking University Cancer Hospital between January 2018 and August 2018. All initial patients included in the study had pathologically confirmed lung cancer and complete clinical and imaging data. Patients were selected for this investigation according to the following inclusion criteria: (I) lung nodule diameters greater than 6 mm; (II) no contraindications to the administration of iodinated contrast materials; (III) age greater than 18 years; and (IV) pathology- and biopsy-confirmed diagnoses of different subtypes of lung cancer confirmed by pathology and biopsy. The exclusion criteria included the following: (I) allergies or contraindications to the administration of iodinated contrast materials; (II) severe liver and renal insufficiency [glomerular filtration rate (GFR) <60 mL/min], thyrotoxicosis, pregnancy, child-bearing age, or lactation; (III) previous therapy including antitumor or anti-inflammatory treatment; and (IV) poor scanning coordination or poor image quality. A total of 85 patients (40 males, 45 females; age range, 42–81 years; mean age, 59.9 years) were enrolled in the current study. All patients underwent scanning with spectral CT perfusion imaging.

Preparation prior to the examination

All patients underwent scanning with spectral CT imaging by a standard protocol. The CT scan was performed during a breath hold following deep inspiration with the patient in the supine position. Before scanning, each patient was instructed on how to breathe during the scan.

CT examination

CT examinations were performed with the patient in the supine position in a Revolution Xtream CT scanner (GE Healthcare, WI, USA). The scanning range was from the apex of the lung to the end of the diaphragmatic surface of the lung bottom; that is, the scanning direction was from head to foot. A plain chest scan was performed first, followed by CT perfusion imaging. Patients were administered contrast material via right median cubital venous access through a bolus injection. Continuous dynamic scanning of the local target lesion was performed 5 s after the start of contrast injection, with a range of 16 mm, lasting for 40 s. The injection flow rate and dose of iohexol (300 mg/mL), a nonionic contrast medium, were similar to those of previous studies (4,5). The injection dose was 40 mL (≤70 kg body weight) at a flow rate of 5 mL/s or 50 mL (>70 kg body weight) at a flow rate of 6 mL/s, followed by 30 mL of saline solution at the same injection rate, which helped reflect the blood perfusion state of the lesion. Acquisition parameters included tube voltage 80/140 kvp, the AutomA technique, a helical pitch of 0.985, a helical tube rotation time of 0.6 s, scan field of view of 500 mm, a collimation zone of 40 mm and a slice thickness of 5 mm. CT Dose Index vol (CTDIvol) for CT perfusion acquisition was of 32.08 mGy.

Quantitative analysis of spectral CT images

By using the Perfusion 4 analysis software with an AW4.7 workstation (GE HealthCare), two senior chest radiologists

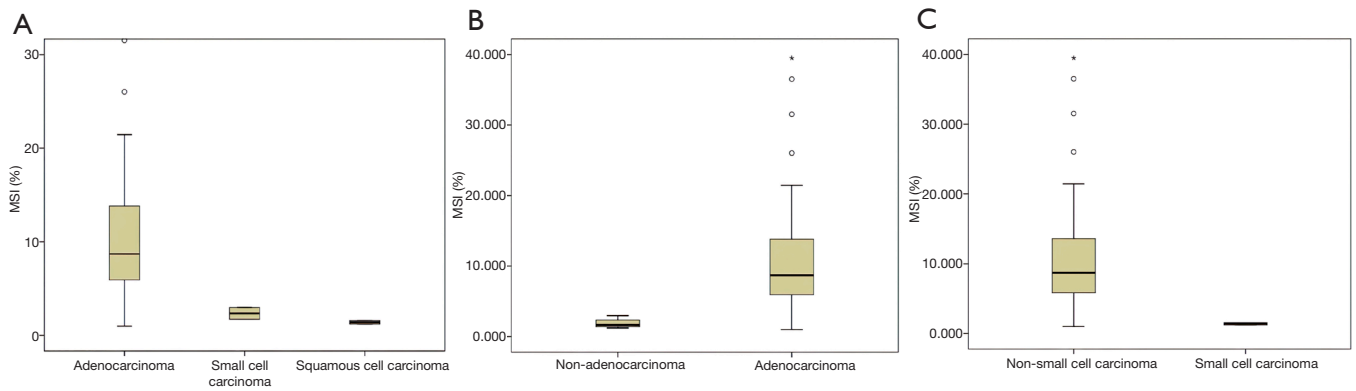

Figure 1 CT perfusion parameters MSI in lung cancers. Circles and asterisks represent outliers statistically. (A) displayed the box plot of CT perfusion parameters MSI in different pathological types of lung cancer. (B) showed the MSI box diagram of adenocarcinoma and non Adenocarcinoma. (C) revealed the MSI box diagram of small cell carcinoma and non-small cell carcinoma. MSI, maximum slope of increase.

analyzed the pulmonary nodule perfusion images, as shown in *Figure 1*. The input artery selected was the aorta or major branch at the same level. The region of interest (ROI) comprising the pulmonary nodule and aorta were selected; to avoid liquefaction, necrosis, hemorrhage, calcification, pulmonary vessels and bronchi, the ROI was made as large as possible at the section showing the maximum size of the lesion and placed with an area of approximately 1/3–2/3 that of the lesion. Average values were obtained by measuring twice at 1-week intervals. The CT perfusion imaging parameters of the ROIs of the lung nodules (*Figure 2*) were obtained: BF, BV, IRF TO, MSI, MTT, PS, PEI, TTP and Tmax.

Pathological evaluation

Pathological specimens were routinely fixed in 10% formalin and embedded in paraffin. Tissue sections were cut at a thickness of 4 μm and stained with hematoxylin and eosin (H&E). Pathological diagnoses were made by two experienced senior pathologists based on the new World Health Organization (WHO) histological classification of lung tumors in 2015 (6).

Statistical analysis

SPSS software (Version 18.0; SPSS Inc., Chicago, IL, USA) was used to perform the statistical analysis. Measurement data are expressed as $\bar{x}\pm s$. First, the quantitative CT perfusion imaging parameters (BF, BV, IRF to, MSI, MTT, PS, PEI, TTP and Tmax) were compared among three groups of lung cancer, including adenocarcinoma, squamous cell carcinoma and small cell lung cancer (SCLC), using one-way analysis of variance (ANOVA) or the Kruskal-Wallis test. Second, the Bonferroni method was used to compare between pairs of groups. Finally, the perfusion parameters were compared between lung adenocarcinoma and non-lung adenocarcinoma and between small cell carcinoma and non-small cell lung cancer (NSCLC). A P value less than 0.05 indicated statistical significance.

Results

Clinical results

Of the eighty-five lung cancer patients, 66 had nonmucinous adenocarcinoma (77.6%), 7 had squamous cell carcinoma (8.2%), 8 had small cell carcinoma (9.4%), and 1 each had mucinous adenocarcinoma, sarcomatoid carcinoma, carcinoid carcinoma and large cell carcinoma (1.2%). All lesions were confirmed by biopsy and surgical pathology.

Comparison of quantitative spectral CT perfusion imaging parameters for lung adenocarcinoma, squamous cell carcinoma and small cell carcinoma

The spectral CT imaging parameters of lung adenocarcinoma, lung squamous cell carcinoma and SCLC are shown in *Tables 1-3* and *Figure 1A,B,C*. Among the different quantitative parameters, MSI was significantly different among adenocarcinoma, squamous cell carcinoma

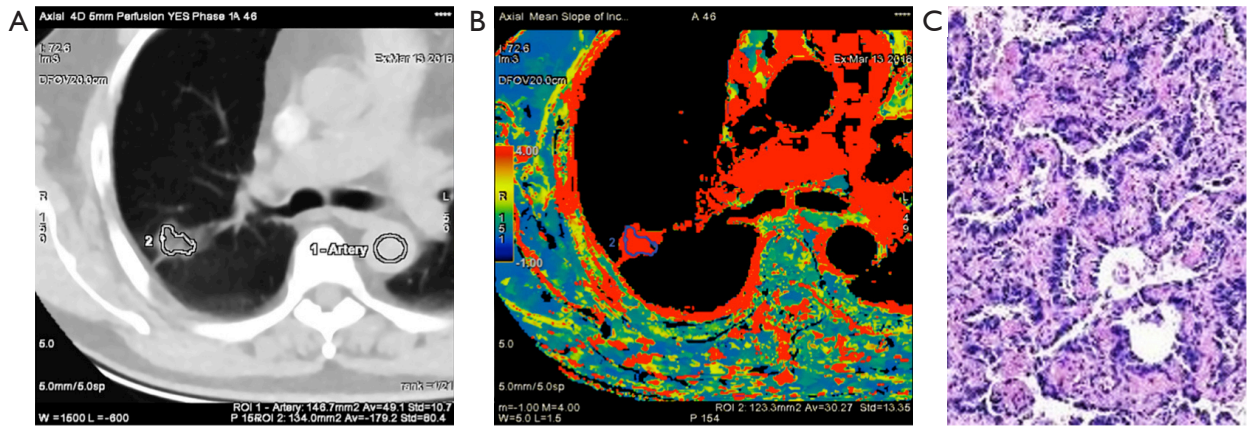

Figure 2 CT perfusion parameter MSI in a 70-year-old male patient with lung adenocarcinoma. (A) Conventional CT showed a mGGN lesion in right upper lobe in a 70-year-old male patient. (B) CT perfusion parameter MSI was 31.1%. (C) The patient was diagnosed with lung adenocarcinoma by pathology [Haematoxylin and eosin (H&E) staining at ×400 magnification)]. MSI, maximum slope of increase; mGGN, mixed ground-glass Nodule; H&E, Haematoxylin and eosin.

Table 1 Comparison of perfusion parameters in adenocarcinomas, squamous cell carcinomas and small cell carcinomas ($\bar{x}$±s)

Parameters	Adenocarcinoma (n=62)	Squamous cell carcinoma (n=3)	Small cell carcinoma (n=5)	P
BF (mL/min/100 g)	63.69±63.49	110.95±32.09	51.89±17.66	0.527
BV (min/100 g)	2.65±2.50	5.40±1.03	4.26±2.17	0.199
IRF T0 (s)	3.51±2.78	1.40±0.28	1.62±0.22	0.239
MSI (%)	11.37±8.74	2.35±0.88	1.40±0.26	0.016
MTT (s)	4.00±3.01	4.82±0.50	7.74±5.77	0.255
PS (mL/min/100 g)	10.00±15.80	17.99±3.18	18.42±4.68	0.538
PEI (HU)	0.34±0.92	0.24±0.17	0.13±0.04	0.344
Tmax (s)	5.10±4.35	3.49±0.35	5.23±3.32	0.837
TTP (s)	17.31±10.31	17.16±2.83	20.72±0.57	0.883

BF, blood flow; BV, blood volume; IRF TO, time of arrival; MSI, maximum slope of increase; MTT, mean transit time; PS, permeability surface area product; PEI, positive enhancement integral; Tmax, time to maximum; TTP, time to peak.

and small cell carcinoma (11.37±8.74 *vs.* 2.35±0.88 *vs.* 1.40±0.26, P=0.016) and decreased gradually across the subtypes, as shown in *Figure 1A* and *Figures 2-4*. There were statistically significant differences in the MSI between lung adenocarcinoma and non-lung adenocarcinoma and between SCLC and NSCLC (P<0.05 for both). The MSI of lung adenocarcinoma was higher than that of NSCLC (11.37±8.74 *vs.* 1.87±0.76, P=0.001), and the MSI of SCLC was lower than that of NSCLC (1.40±0.26 *vs.* 10.77±6.72, P=0.014). However, there was no significant difference in any of the spectral CT parameters between SCLC and lung squamous cell carcinoma (P>0.05).

Discussion

Primary lung cancer has the highest incidence among cancers worldwide (7). It is also the deadliest form of cancer in China (8). According to the WHO in 2015, the three most common types of lung cancer are adenocarcinoma, squamous cell carcinoma and small cell carcinoma (6). Different pathological types of lung cancer have different biological behaviors and treatment plans. A pathological diagnosis is the basis for developing a reasonable treatment plan and assessing prognosis. Traditional chest CT is used to infer the pathological type of lung cancer, mainly based

Table 2 Comparison of perfusion parameters in small cell carcinomas and non-small cell carcinomas ($\bar{x}$±s)

Parameters	Non-small cell carcinoma (n=65)	Small cell carcinoma (n=5)	P
BF (mL/min/100 g)	66.05±55.87	51.89±17.66	0.794
BV (min/100 g)	2.75±2.27	4.26±2.17	0.376
IRF T0 (s)	4.69±2.58	1.62±0.22	0.337
MSI (%)	10.77±6.72	1.40±0.26	0.014
MTT (s)	4.96±3.36	7.74±5.77	0.244
PS (mL/min/100 g)	14.88±16.31	18.42±4.68	0.362
PEI (HU)	0.27±0.37	0.13±0.04	0.603
Tmax (s)	6.39±3.88	5.23±3.32	0.819
TTP (s)	18.60±10.43	20.72±0.57	0.489

BF, blood flow; BV, blood volume; IRF TO, time of arrival; MSI, maximum slope of increase; MTT, mean transit time; PS, permeability surface area product; PEI, positive enhancement integral; Tmax, time to maximum; TTP, time to peak.

Table 3 Comparison of parameters in adenocarcinomas and non-adenocarcinomas ($\bar{x}$±s)

Parameters	Adenocarcinoma (n=62)	Non-adenocarcinoma (n=8)	P
BF (mL/min/100 g)	63.69±63.49	81.42±40.11	0.237
BV (min/100 g)	2.65±2.50	4.83±1.53	0.054
IRF T0 (s)	3.51±2.78	1.51±0.24	0.098
MSI (%)	11.37±8.74	1.87±0.76	0.001
MTT (s)	4.00±3.01	6.28±3.74	0.126
PS (mL/min/100 g)	10.00±15.80	18.20±3.68	0.562
PEI (HU)	0.34±0.92	0.19±0.12	0.171
Tmax (s)	5.10±4.35	4.36±2.17	0.247
TTP (s)	17.31±10.31	18.94±2.64	0.871

BF, blood flow; BV, blood volume; IRF TO, time of arrival; MSI, maximum slope of increase; MTT, mean transit time; PS, permeability surface area product; PEI, positive enhancement integral; Tmax, time to maximum; TTP, time to peak.

on clinical experience. Adenocarcinoma is a peripheral lung cancer, while small cell carcinoma and squamous cell carcinoma are central cancers; in the early stage, small cell carcinoma often presents with hilar and mediastinal lymph node metastases; squamous cell carcinoma is prone to necrosis and cavity formation; and some early-stage adenocarcinomas exhibit ground glass opacities. In addition, the value of enhanced CT is limited in the differential diagnosis of different pathological types of lung cancer. Dynamic contrast-enhanced ultrasound or MRI is not an ideal option for the assessment of lung tumors because of the restriction to acoustic windows or scanning speed. However, CT perfusion imaging can evaluate the hemodynamic changes in tumors (4) and may be aid in the pathological and differential diagnosis of lung cancer through quantitative multiparameter analysis (5,9-15). Most of previous CT perfusion research is generally obtained through a bolus injection of contrast agent at a simple injection rate of at least 4 mL/s (from 4 to 8 mL/s) and a single injected iodine dose within the range of 12–18 g (about 20–60 mL of total iodinated contrast medium) for different studies with ignoring the relationship of injection rate, dose and weight. The injection dosage and speed were adjusted according to different body weights for more accurate and stable data in our study.

In this study, we compared the spectral CT perfusion

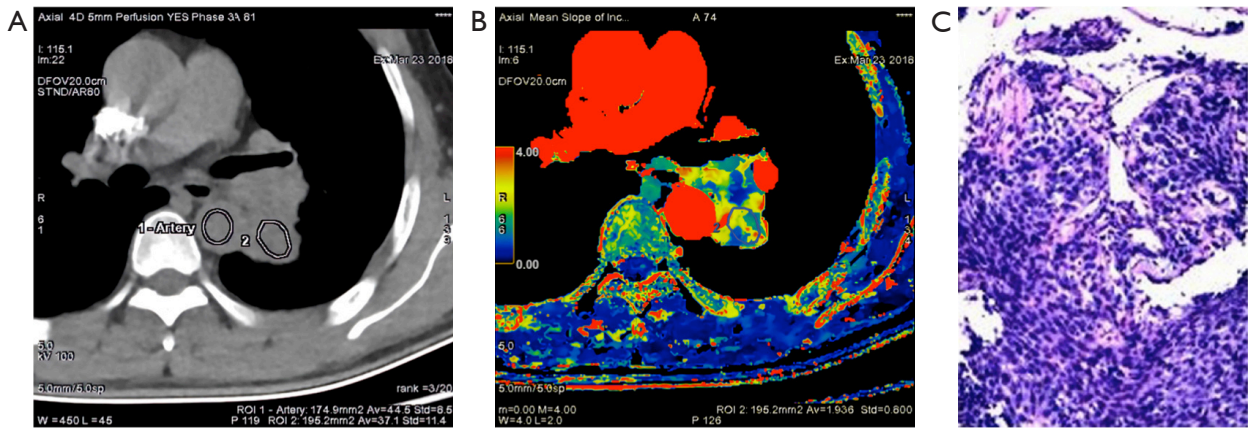

Figure 3 CT perfusion parameter MSI in a 69-year-old male patient with squamous cell lung cancer. (A) Conventional CT examined a nodule in left upper lobe in a 69-year-old male patient. (B) CT perfusion parameter MSI was 1.66%. (C)The pathological specimen revealed squamous cell lung cancer (H&E staining at ×400 magnification). MSI, maximum slope of increase; H&E, Haematoxylin and eosin.

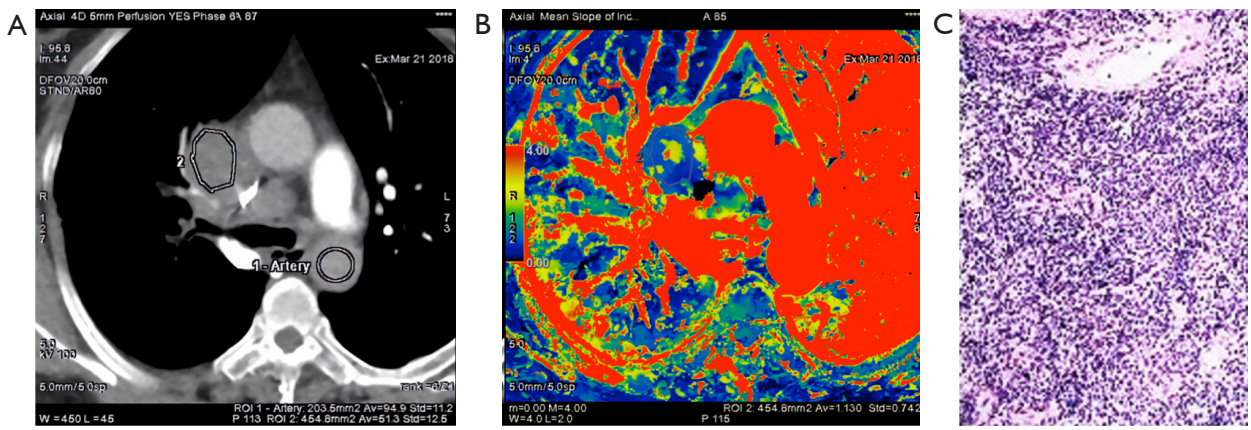

Figure 4 CT perfusion parameter MSI in a 52-year-old female patient with small cell lung cancer. (A) Conventional CT showed a mass in right upper lobe in a 52-year-old female patient. (B) CT perfusion parameter MSI was 1.13%. (C) Small cell lung cancer was confirmed by pathology (H&E staining at ×400 magnification). MSI, maximum slope of increase; H&E, Haematoxylin and eosin.

imaging parameters of different pathological types of lung cancer and found that the MSI was significantly different among adenocarcinoma, squamous cell carcinoma and small cell carcinoma. The MSI of adenocarcinoma was higher than that of squamous cell carcinoma and small cell carcinoma (*Figure 1 vs. Figure 2*). Moreover, when adenocarcinoma and non-adenocarcinoma were compared, the MSI of adenocarcinoma was higher than that of non-adenocarcinoma. In terms of histopathology, adenocarcinoma mostly exhibits adenoid differentiation and tubular or glandular structures, while small cell carcinoma and squamous cell carcinoma have dense internal cells and structures, and squamous cell carcinoma often further exhibits tumor nests, keratinized beads or intercellular bridges. In addition, the proportions of tumor parenchyma and stroma among adenocarcinoma, squamous cell carcinoma and small cell carcinoma lead to differences in structure, density, degree of blood perfusion and retention time, which may be reflected by the MSI. The blood perfusion speed of adenocarcinoma is greater than that of lung squamous cell carcinoma and small cell carcinoma. The only similar research was performed by Wang and coworkers (16), who reported pathological subtypes of lung cancer with spectral CT parameters. After a comparative study of 29 patients with squamous cell carcinoma and 15 with adenocarcinoma, they found that the slope of the

spectral attenuation characteristic curve and the single-energy CT values at 40 keV of adenocarcinoma were higher than those of squamous cell carcinoma. This study indicated that the net CT enhancement value for lung adenocarcinoma at the arterial phase was higher than that for squamous cell carcinoma, which might also indirectly prove that the enhancement rate of adenocarcinoma is higher than that of squamous cell carcinoma. This might explain why the maximum ascending slope of adenocarcinoma was higher than that of squamous cell carcinoma. The pathological explanation may be that adenocarcinoma is prone to form abundant and uniform sieves, such as capillaries, and that its tumor microvessel density is higher than that of squamous cell carcinoma, which more easily forms solid masses (17-20). The microvessel density of the tumor directly reflects the tumor blood supply and affects the enhancement degree and speed of the CT contrast agent. Therefore, the MSI, reflecting the CT perfusion velocity, of adenocarcinoma is higher than that of squamous cell carcinoma. However, previous studies by other pathologists demonstrated that the microvessel density of NSCLC was often lower than that of SCLC, which seems to be inconsistent with the results of this study. The reason for this discrepancy might be that the specimens of the pathological study were all solid masses, while in our study, ground glass opacities were observed in 61.2% (41/67) of the nodules, most with adherent growth, which could easily lead to the formation of abundant tumor microvessels and faster blood perfusion. In addition, there are no effective spectral CT perfusion imaging parameters that can reflect the difference in blood perfusion between lung squamous cell carcinoma and small cell carcinoma, which may also reflect that there is no significant difference between the two types of cancer.

Theoretically, the different pathological tissue components of lung squamous cell carcinoma, lung adenocarcinoma and small cell carcinoma should also have different hemodynamic characteristics, and the corresponding CT perfusion imaging parameters should have certain differences. In this study, we found that only MSI was different among the different pathological types of lung cancer. Our study has several limitations. Our sample had a certain bias, with few patients with small cell carcinoma and squamous cell carcinoma. Although this is related to the epidemiology of lung cancer itself, this unbalanced sample size was nevertheless a concern. Another limitation was the disproportion of ground glass opacities and solid densities among the lung cancers, which might affect the stability of the results. Therefore, it will be necessary to increase the sample size and perform stratified analyses on solid lung lesions and ground glass lung adenocarcinoma to obtain more reliable research results.

Conclusions

In conclusion, spectral CT perfusion imaging techniques have an important role in the differential diagnosis of different pathological types of lung cancer. There were significant differences in the MSI among adenocarcinoma, squamous cell carcinoma and small cell carcinoma; specifically, the MSI of adenocarcinoma was higher than that of both squamous cell carcinoma and small carcinoma. MSI may play a significant role in the diagnosis of different pathological types of lung cancer, which may be revealed through future in-depth studies with larger sample sizes.

Acknowledgments

Funding: This study was supported by 2019 SKY Imaging Research Fund of the Chinese International Medical Foundation (Project No. Z-2014-07-1912), Beijing Natural Science Foundation (Z200015), Beijing Municipal Administration of Hospitals Clinical Medicine Development of Special Funding Support (No. ZYLX201803), Beijing Hospitals Authority' Ascent Plan (DFL20191103), the third round of public welfare development and reform pilot projects of Beijing Municipal Medical Research Institutes (Beijing Medical Research Institute, 2019-1).

Footnote

Reporting Checklist: The authors have completed the MDAR checklist. Available at https://dx.doi.org/10.21037/tcr-20-3479

Data Sharing Statement: Available at https://dx.doi.org/10.21037/tcr-20-3479

Conflicts of Interest: All authors have completed the ICMJE uniform disclosure form (available at https://dx.doi.org/10.21037/tcr-20-3479). The authors have no conflicts of interest to declare.

Ethical Statement: The authors are accountable for all aspects of the work in ensuring that questions related to the accuracy or integrity of any part of the work are appropriately investigated and resolved. The study was conducted in accordance with the Declaration of Helsinki (as

revised in 2013). The study was approved by the Medical Ethics Committee of Peking University Cancer Hospital & Institute (NO.: 2021KT04), and written informed consent was obtained from all patients.

References

1. Ohno Y, Nishio M, Koyama H, et al. Dynamic contrast-enhanced CT and MRI for pulmonary nodule assessment. AJR Am J Roentgenol 2014;202:515-29.
2. Mirsadraee S, van Beek EJ. Functional imaging: computed tomography and MRI. Clin Chest Med 2015;36:349-63, x.
3. Chen ML, Sun YS. CT perfusion imaging: a valuable and feasible resolution of pulmonary nodules. Advanced Ultrasound in Diagnosis and Therapy 2019;02:027-034.
4. Bohlsen D, Talakic E, Fritz GA, et al. First pass dual input volume CT-perfusion of lung lesions: The influence of the CT-value range settings on the perfusion values of benign and malignant entities. Eur J Radiol 2016;85:1109-14.
5. Ohno Y, Koyama H, Fujisawa Y, et al. Dynamic contrast-enhanced perfusion area detector CT for non-small cell lung cancer patients: influence of mathematical models on early prediction capabilities for treatment response and recurrence after chemoradiotherapy. Eur J Radiol 2016;85:176-86.
6. Travis WD, Brambilla E, Nicholson AG, et al. The 2015 World Health Organization Classification of Lung Tumors: Impact of Genetic, Clinical and Radiologic Advances Since the 2004 Classification. J Thorac Oncol 2015;10:1243-60.
7. Torre LA, Bray F, Siege RL, et al. Global cancer statistics, 2012. CA Cancer J Clin 2015;65:87-108.
8. Chen W, Zheng R, Baade PD, et al. Cancer statistics in China, 2015. CA Cancer J Clin 2016;66:115-32.
9. Kiessling F, Boese J, Corvinus C, et al. Perfusion CT in patients with advanced bronchial carcinomas: a novel chance for characterization and treatment monitoring? Eur Radiol 2004;14:1226-33.
10. Li Y, Yang ZG, Chen TW, et al. First-pass perfusion imaging of solitary pulmonary nodules with 64-detector row CT: comparison of perfusion parameters of malignant and benign lesions. Br J Radiol 2010;83:785-90.
11. Sitartchouk I, Roberts HC, Pereira AM, et al. Computed tomography perfusion using first pass methods for lung nodule characterization. Invest Radiol 2008;43:349-58.
12. Shan F, Zhang Z, Xing W, et al. Differentiation between malignant and benign solitary pulmonary nodules: use of volume first-pass perfusion and combined with routine computed tomography. Eur J Radiol 2012;81:3598-605.
13. Shu SJ, Liu BL, Jiang HJ. Optimization of the scanning technique and diagnosis of pulmonary nodules with first-pass 64-detector-row perfusion VCT. Clin Imaging 2013;37:256-64.
14. Lee YH, Kwon W, Kim MS, et al. Lung perfusion CT: the differentiation of cavitary mass. Eur J Radiol 2010;73:59-65.
15. Ma SH, Le HB, Jia BH, et al. Peripheral pulmonary nodules: relationship between multi-slice spiral CT perfusion imaging and tumor angiogenesis and VEGF expression. BMC Cancer 2008;8:186.
16. Wang G, Zhang C, Li M, et al. Preliminary application of high-definition computed tomographic Gemstone Spectral Imaging in lung cancer. J Comput Assist Tomogr 2014;38:77-81.
17. Zieliński KW, Kulig A. Morphology of the microvascular bed in primary human carcinomas of lung. Part I: Three--dimensional pattern of microvascular network. Pathol Res Pract 1984;178:243-50.
18. Zieliński KW, Kulig A, Zieliński J. Morphology of the microvascular bed in primary human carcinomas of lung. Part II. Morphometric investigations of microvascular bed of lung tumors. Pathol Res Pract 1984;178:369-77.
19. Yuan A, Yu CJ, Kuo SH, et al. Vascular endothelial growth factor 189 mRNA isoform expression specifically correlates with tumor angiogenesis, patient survival, and postoperative relapse in non-small cell lung cancer. J Clin Oncol 2001;19:432-41.
20. Lucchi M, Mussi A, Fontanini G, et al. Small cell lung carcinoma (SCLC): the angiogenic phenomenon. Eur J Cardiothorac Surg 2002;21:1105-10.

Cite this article as: Chen ML, Wei YY, Li XT, Qi LP, Sun YS. Low-dose spectral CT perfusion imaging of lung cancer quantitative analysis in different pathological subtypes. Transl Cancer Res 2021;10(6):2841-2848. doi: 10.21037/tcr-20-3479

